IRCTR DRIZZLE RADAR

- IDRA -

DATASET DESCRIPTION DOCUMENT FOR THE CDS DATASETS

<cesar_idra_products_lb1_t00_v1.0>

TU Delft Delft University of Technology

Table of Contents

Document Status

*status)**	*name*	*organisation*	*date*	*signature*
prepared	T. Otto	TUD	2012-11-20	

) prepared, checked, approved, authorized, accepted.*

document title : DDS for the CDS datasets <cesar_idra_products_lb1_t00_v1.0>			
document reference id: cesar_idra_products_lb1_t00_v1.0.pdf			
version	*author*	*date*	*reason for change*
0.1	T. Otto	2012-11-20	draft
1.0	T. Otto	2012-11-26	completion of the document

Quick Facts

Dataset Content:

- *instantaneous rainfall rate* (R) estimated from measurements of the horizontally scanning polarimetric radar IDRA for the area around CESAR, available for:

  minimum range from the tower = 210 m
  maximum range from the tower = 15360 m

  in the radar-centred polar coordinate system (range and azimuth), based on the following two IDRA observables applying fixed parameterisations based on

- *specific differential phase* (KDP) which is
  - independent of radar calibration and signal attenuation,
  - estimated applying a novel method that overcomes the poor range resolution of conventional methods to estimate KDP, [iv].

- *reflectivity corrected for gaseous and rain attenuation* (Z)
  - used to estimate the rainfall rate when KDP is not available, i.e. usually for weak instantaneous rainfall rates approx. < 3 mmh^{-1}.

- additional variables of this dataset
  - *differential backscatter phase*,
  - *standard deviations* of all observables accounting for the measurement uncertainties,
  - *daily rain accumulation* as displayed on the quicklook, and
  - *data processing flags*.

Data Policy:

- the CESAR data policy applies: http://www.cesar-database.nl/DataPolicy.do

- if you use the data in a scientific publication, please cite it using the digital object identifier of IDRA data in the 3TU.Datacentre, e.g.

  T. Otto and H.W.J. Russchenberg, 2010: IDRA weather radar measurements – all data, TU Delft, Dataset, http://dx.doi.org/10.4121/uuid:5f3bcaa2-a456-4a66-a67b-1eec928cae6d.

Useful Resources:

- this document and the references cited within,

- short course on radar meteorology (online lecture)
  http://collegerama.tudelft.nl/mediasite/SilverlightPlayer/Default.aspx?peid=1805993fac954c3fba5855bce7e6a86e1d

- introduction to weather radar polarimetry and X-band peculiarities (online lecture)
  http://collegerama.tudelft.nl/Mediasite/Play/e6924e44ad014a16ac99b1e2464b98001d?catalog=7b5b0161-423f-43b2-851f-4b90fd27d07f

Application Notes:

- *daily rain accumulation* (shown on the quicklook)
  - is based on the rainfall rate estimates by IDRA, therefore, it includes only rain periods when IDRA was actually measuring, and no issues such as a synchronisation loss occurred; please check the Section Data Quality for details.

- *instantaneous rainfall rate*
  - estimated based on Z-R and KDP-R relations as outlined in the Section Data Processing,
  - fixed parameterisations of Z-R and KDP-R used, however, KDP and Z are available in this dataset such that any other parameterisation can be easily applied,
  - data are provided in the radar-centred polar coordinate system, for the radar position (latitude/longitude/altitude and Rijksdriehoekscoördinaten EPSG:28992 Amersfoort) please refer to the Section Specifications,
  - consider that the radar measurements only provide "snapshots" of the spatial distribution of precipitation, for IDRA, every minute a new snapshot is provided, its antennas rotate with a speed of one round per minute,

    for fast-evolving convective storms with a high-spatial variability, this temporal resolution might not be sufficient,

    e.g. consider horizontal wind speeds in the order of 15 ms^{-1} which results in a horizontal displacement of precipitation of 900 m in one minute (the revisit time of IDRA), therefore, a small heavy precipitating core might not be sampled by IDRA at all locations it is actually passing, the result is a wavy pattern in rain accumulation if the rain rates measured by IDRA are considered to be constant for one minute until revisiting (this assumption is applied for the creation of the accumulated rain map that is shown on the quicklook of this dataset),

    depending on your application, you might consider to apply cell tracking algorithms or temporal interpolation schemes, i.e. advection correction methods, to reduce this effect,

    the corresponding Doppler velocity data are available in the dataset <IDRA_yyyy_mm_dd_standard_range.nc> at [iii].

- *specific differential phase* and *differential backscatter phase*
  - usually the processing of the measured differential phase concentrates on the suppression of the differential backscatter phase, and the extraction of the propagation phase (specific differential phase) only,

    actually, the differential backscatter phase is a very attractive weather radar observable because it has the same advantages as the specific differential phase, namely its independence of signal attenuation and radar calibration, but it shows a different sensitivity with respect to the drop-size distribution, i.e. it is independent of the concentration parameter,
  - these properties make the differential backscatter phase a prime observable for drop-size distribution retrieval at X-band, [6], [7],
  - the differential backscatter phase is also an indicator of Mie-scattering, i.e. it shows the presence of raindrops with diameters larger than 3 mm at X-band frequencies.

General Overview

This dataset description document provides information for the CDS datasets
cesar_idra_products_lb1_t00_v1.0.

IDRA is the TU Delft IRCTR drizzle radar that is located on top of the Cabauw tower, 213 m agl., since October 2007, Figure 1. IDRA is a polarimetric X-band (9.475 GHz, horizontal/vertical polarisations) FMCW radar developed at Delft University of Technology. Its antennas rotate at 1 rpm at a fixed low elevation angle providing *high-resolution observations of the horizontally spatial and temporal distribution of precipitation up to a range of 15.36 km around the Cabauw Site for Atmospheric Research (CESAR).* The radar transmits linear sawtooth frequency modulated sweeps alternately at horizontal and vertical polarisation. The backscattered signal is received simultaneously in an horizontally and a vertically polarised channel.

Figure 1: IDRA on top of the Cabauw tower. IDRA uses two antennas, one for transmit and one for receive.

The central frequency of 9.475 GHz, sensitive receivers with a large dynamic range, and the possibility to adjust the power of the transmitted signal, permit IDRA to monitor the spatial distribution and the temporal evolution of precipitation (from fog and drizzle to heavy convective rain).

This dataset contains the following IDRA products as a result of a post-processing of IDRA standard range (max. 15.36 km) data available at the 3TU.Datacentre [iii]:

- reflectivity corrected for rain- and gaseous attenuation Z_{hh} (dBZ),
- specific differential phase K_{dp} (deg km^{-1}) and its standard deviation,
- differential backscatter phase δ_{co} (deg) and its standard deviation,
- estimated rainfall rate (mm h^{-1}) and its standard deviation,
- daily rain accumulation (mm) as displayed on the quicklook,
- data processing flags.

The dataset is available in the NetCDF format according to the requirements of the CESAR database system. The metadata is compliant with the "netCDF Climate and Forecast Metadata Convention - CF1.4", see [2] and [3] for further information.

The CESAR data policy applies which can be found online at http://www.cesar-database.nl. If this data is used in a scientific publication please cite it using the digital object identifier (DOI) of IDRA data in the 3TU.Datacentre:

> T. Otto and H.W.J. Russchenberg, 2010: *IDRA weather radar measurements – all data*, TU Delft, Dataset, http://dx.doi.org/10.4121/uuid:5f3bcaa2-a456-4a66-a67b-1eec928cae6d.

Contacts

Principle Investigator (PI)

Name: Tobias Otto
Herman Russchenberg

Address: TU Delft Climate Institute
Department of Geoscience and Remote Sensing
Stevinweg 1
2628 CN Delft
The Netherlands

Tel.: +31 (0)15 27 87603

E-Mail: t.otto@tudelft.nl
h.w.j.russchenberg@tudelft.nl

Instrument Developer

Name: Jordi Figueras i Ventura (Instrument Developer)
Fred van der Zwan (Technical staff)
Paul Hakkaart (Technical staff)
Johan Zijderveld (Technical staff)

Address: International Research Centre for Telecommunications and Radar - IRCTR
Delft University of Technology
Mekelweg 4
2628 CD Delft
The Netherlands

Deployment Locations and History

IDRA is a stationary radar system, installed on top of the Cabauw tower. The following list gives an overview when IDRA was installed at the Cabauw tower, and in which periods IDRA was operational (green marker).

August 2007	Installation of IDRA on top of the Cabauw tower.
18-10-2007	First measurement, antenna stationary.
05-12-2007	First measurement with rotating antennas.
14-12-2007	Installation of the IDRA control and data processing computer.
26-06-2008	The real-time processing reaches operational status.
28-11-2008	IDRA's electronics were removed from the tower to improve the receivers.
05-03-2009	IDRA's electronics were re-installed on the tower.
27-04-2009	IDRA is fully operational again.
09-12-2009	*Signal processing changed*, see Section "Signal Processing" for details.
26-12-2009	Mechanical problems with the antenna gear box.
01-01-2010	Antenna gear-box problem solved. IDRA is back to normal operation. Estimated rainfall rate retrievals available at the CESAR database from this date onwards.

Near-Real-Time Data Plots

Near-real-time data plots of IDRA measurements can be found online at:

http://ftp.tudelft.nl/TUDelft/irctr-rse/idra/

IDRA's near-real-time plots are updated once per minute.

Data Description and Examples

Figure 2 shows one-minute of data which corresponds to one full antenna rotation, i.e. to one plan-position indicator (PPI). The radar is located in the middle of the plots. The ordinate and the abscissa of this PPI show the range (km) from the radar.

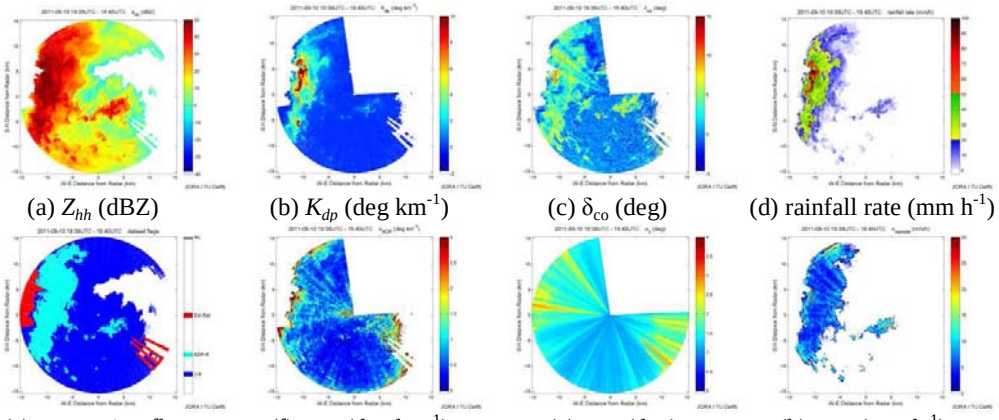

(a) Z_{hh} (dBZ) (b) K_{dp} (deg km^{-1}) (c) δ_{co} (deg) (d) rainfall rate (mm h^{-1})

(e) processing flags (f) σ_{kdp} (deg km^{-1}) (g) $\sigma_{\delta co}$ (deg) (h) σ_{rain} (mm h^{-1})

Figure 2: Primary variables of this dataset. See explanation below for details.

Shown are the primary variables of this dataset, namely:

Fig. 2(a): Co-polarised equivalent reflectivity factor at horizontal polarisation corrected for gaseous- and rain attenuation Z_{hh} (dBZ). The reflectivity in linear units (mm^6·m^{-3}) is proportional to the backscattered and received power.

Fig. 2(b): Estimated one-way specific differential phase K_{dp} (deg km^{-1}), and corresponding standard deviation σ_{kdp} (deg km^{-1}) shown in Fig. 2(f).

Fig. 2(c): Estimated differential backscatter phase (deg), and corresponding standard deviation $\sigma_{\delta co}$ (deg) shown in Fig. 2(g).

Fig. 2(d): Estimated instantaneous rainfall rate (mm h^{-1}), and corresponding standard deviation σ_{rain} (mm h^{-1}) shown in Fig. 2(h).

Fig. 2(e): Data processing flags with the following possible values

- 0 - no flags,
- 1 - rainfall rate estimate based on Z-R relation,
- 2 - rainfall rate estimate based on KDP-R relation,
- 4 - no rainfall rate estimation due to total signal extinction or receiver saturation,
- 8 - no rainfall rate estimation, radar measurements likely whithin or above the melting layer.

The data are in radar-centred polar coordinates (radar azimuth and range).

In irregular intervals, data might be missing. Missing data may indicate that IDRA was not running in the standard-range mode but in a different mode, or that IDRA was not measuring at all. For a query whether missing data are available in a different data acquisition mode for a specific date check the quicklooks of IDRA data available at the 3TU.Datacentre, [iii], or contact the PI.

Data File Contents

Table 1 provides an overview of the dimensions, global attributes, and variables contained of the dataset. For additional information on dimensions and variables please refer to their corresponding *units* and *comment* attributes.

Note that most primary variables are stored as 16-bit integer. They need to be multiplied by their corresponding *scale_factor* attribute! For the *rainfall_rate* and *sigma_rainfall_rate*, also their corresponding *add_offset* attributes need to be applied:

$$unpacked\_value = packed\_value \cdot scale\_factor + add\_offset.$$

Table 1: < cesar_idra_products_lb1_t00_v1.0> contents.

Dimensions	**Description**
scalar	dimension used for variables with one value
time	time dimension
range	range dimension
quicklook_azimuth	azimuth dimension used only for the primary variable *thickness_of_daily_rainfall_amount*
Attributes	**Description**
global attributes	as specified by [2]
Primary variables	**Description**
equivalent_reflectivity_factor	co-polarised equivalent reflectivity factor at horizontal polarisation Z_{hh} (dBZ) corrected for gaseous- and rain attenuation; ☝ *scale_factor* attribute applies
specific_differential_phase	specific differential phase K_{dp} (deg km^{-1}); ☝ *scale_factor* attribute applies
sigma_specific_differential_phase	standard deviation of the specific differential phase σ_{kdp} (deg km^{-1}); ☝ *scale_factor* attribute applies
differential_backscatter_phase	differential backscatter phase δ_{co} (deg); ☝ *scale_factor* attribute applies
sigma_differential_backscatter_phase	standard deviation of the differential backscatter phase $\sigma_{\delta co}$ (deg); ☝ *scale_factor* attribute applies
rainfall_rate	instantaneous rainfall rate (mm h^{-1}); ☝ *scale_factor* and *add_offset* attribute applies
sigma_rainfall_rate	standard deviation of the rainfall rate σ_{rain} (mm h^{-1}), only for rainfall rates estimates based on *specific_differential_phase* (KDP-R relation) ☝ *scale_factor* and *add_offset* attribute applies
dataset_flags	data processing flags: 0 - no flags, 1 - rainfall rate estimate based on Z-R relation, 2 - rainfall rate estimate based on KDP-R relation, 4 - no rainfall rate estimation due to total signal extinction or receiver saturation, 8 - no rainfall rate estimation, radar measurements likely whithin or above the melting layer.
thickness_of_daily_rainfall_amount	daily rainfall accumulation (m) as displayed on the quick-look

Secondary variables	Description
iso_dataset	contains a copy of the dataset metadata, for more information refer to [2]
product	contains a copy of the product metadata, for more information refer to [2], and additional metadata of the dataset
station_details	contains metadata describing station details, for more information refer to [2]
azimuth[1]	azimuth angle of each profile (rad), applies to each primary variable except *thickness_of_daily_rainfall_amount*. It must be stressed that there is no fixed partition of one scan (one plan-position indicator) into regular angular intervals because the data acquisition rate is not synchronised with the antenna rotation speed of one round per minute. Therefore, each profile is tagged with its *azimuth*.
gaseous_attenuation	gaseous attenuation (dB) applied to correct *equivalent_reflectivity_factor* for gaseous attenuation
range_resolution	the resolution along slant range (m)
frequency_excursion	bandwidth of the transmitted linear up-chirp (Hz)
differential_phase_offset	system differential phase offset that is applied to the measured differential phase in order to correctly estimate the differential backscatter phase, see Section Data Processing for details

[1] IDRA's antennas rotate at one round per minute.
This dataset is acquired in the alternate polarization mode, with a sweep time of 409.6 μs. Therefore, the measurement of one polarimetric cycle requires 2x409.6 μs = 819.2 μs. For one profile, 512 polarimetric cycles are averaged, 512x819.2 μs = 0.4194304 s. A total of 143 profiles does not cover one full plan-position indicator but only 359.81° as it takes 59.9785472 s which is less than the 60 s time for one full antenna rotation.

Primary Variables and Expected Uncertainty

For the primary variables *specific_differential_phase*, *differential_backscatter_phase*, and *rainfall_rate*, the uncertainty is quantified by the corresponding standard deviation provided by the primary variables *sigma_differential phase*, *sigma_differential_backscatter_phase*, and *sigma_rainfall_rate*, respectively.

These standard deviations do account for measurement uncertainties. However, they do not account for the following uncertainties and possible systematic errors:

differential_backscatter_phase:
The differential backscatter phase is derived as the difference of the measured differential phase and the differential propagation phase (twice the range accumulation of the specific differential phase). In case the system differential phase (secondary variable *differential_phase_offset*) is not properly estimated, the differential backscatter phase will be biased.

rainfall_rate:
The provided standard deviation of the rainfall rate only accounts for the measurement uncertainty. However, be aware that for the estimation of the rainfall rate, Z-R and KDP-R relations with fixed parameterisations are employed that are valid for one raindrop-size distribution only. The *rainfall_rate* will thus be biased due to natural variability of the raindrop-size distribution. This bias is more significant in case the Z-R relation is employed, see Figure 3.

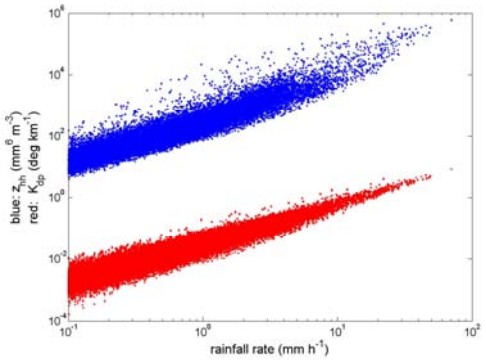

Figure 3: X-band scattering computations based on a large variety of raindrop-size distributions measured over two years by a 2D-video disdrometer at CESAR. Especially for higher rainfall rates, it can be seen that the variability of Z-R (blue) is much larger than the variability of KDP-R (red). KDP-R relations are usually employed at X-band frequencies for instantaneous rainfall rates >3 mm h^{-1}.

In addition rainfall rates estimated by the Z-R relation can be biased due to an over- or under-compensation for gaseous- and rain-attenuation, or due to radar mis-calibration. Because K_{dp} is independent of signal attenuation, and furthermore it is a self-calibrating measurement, rainfall rates estimated by the KDP-R relation are not affected by those issues. The primary variable *dataset_flags* provides information whether the *rainfall_rate* is based on the *equivalent_reflectivity_factor* (Z-R relation) or on the *specific_differential_phase* (KDP-R relation).

For more detailed information, the reader is referred to the Section Data Processing and references provided therein.

Quicklook

The quicklook shows a PPI of the daily rain accumulation *RRd* (mm) based on the IDRA measurements, i.e.

$$RRd(range, azimuth) = \sum_{time} RR(range, azimuth) \cdot \Delta t$$

where Δt is the update rate of the rainfall rate *RR* measurements by IDRA, i.e. one minute. The daily rain accumulation is also stored in the dataset as the primary variable *thickness_of_daily_rainfall_amout*.

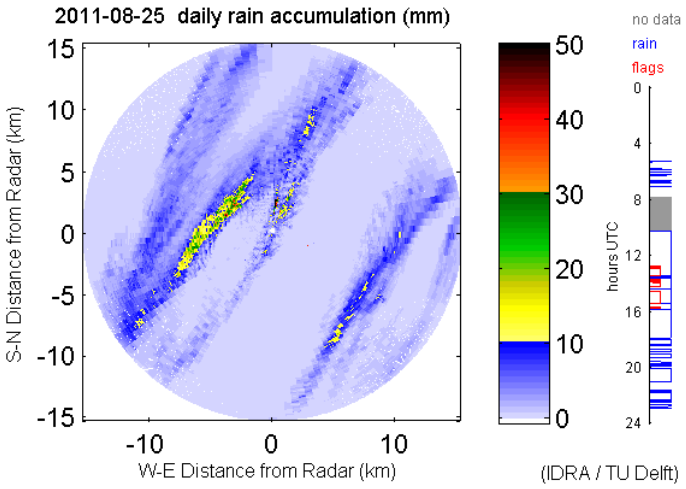

Figure 4: Example of a quicklook.

Be aware that the daily rain accumulation is based on IDRA data only, if there were periods during the day when IDRA was not measuring in the standard mode, the daily rain accumulation might not correspond to the true daily rain accumulation. Also in case of a synchronisation loss, IDRA might miss rain, see Section Data Quality → Synchronisation Loss for details.

An indicator which periods during a day were taken into account for the computation of the daily rain accumulation is shown right next to the PPI (blue curve). Also shown are periods when no data was acquired in the standard mode (grey shaded area).

To check whether IDRA missed some rain, please compare the quicklook information with either the CESAR rain gauge measurements provided at the http://www.cesar-database.nl, or with measurements of the KNMI weather radars that are accessible e.g. via http://www.buienradar.nl/historie.aspx (note that this website uses Central European Time instead of UTC).

An additional indicator (the red curve) shows the presence of processing flags, i.e. whether in a certain period certain range-bins were not used for the rainfall rate estimation due to total signal extinction, radar receiver saturation or possible measurements in or above the melting layer, see the Section Data Quality for more information.

Data Processing

This dataset is based on the polarimetric moments: attenuated reflectivity, attenuated differential reflectivity, and differential phase measured by IDRA, and made publicly available through the 3TU.Datacentre, [iii]. For details about IDRA and the signal processing (e.g. clutter filter) employed, please refer to the dataset description document of the data in the 3TU.Datacentre, [4], and for more detailed information to [i].

Only IDRA data after December 2009 is processed because the signal processing was changed back then. This decision was made due to the fact that the previous signal processing was optimised for the observation of drizzle and light rain (i.e. a spectral clutter filter based on the differential reflectivity and the differential phase was employed which also partially suppressed radar signals from heavy precipitation).

The following processing steps are applied to estimate the primary variables of this dataset:

1. Based on the quicklook data available at the 3TU.Datacentre, [iii] (<IDRA_yyyy-mm-dd_quicklook>), a rain mask is derived for IDRA measuring in the standard mode (15.36 km max. range at a range resolution of 30 m). The rain mask is shown as a blue curve on the dataset quicklook.
   Only data that falls within the rain mask is used for further processing.

2. Based on the radiosounding (De Bilt) at 00:00UTC, 12:00UTC, and 24:00UTC, and the temperature measurements of the CESAR tower, the approximate lower height of the melting layer is estimated.
   IDRA data that might be contaminated by measurements within or above the melting layer is removed from the further processing.
   The primary variable *dataset_flags* is set to the value *8* when this is the case.

3. A speckle filter based on morphological image processing is applied in order to remove spikes and single range-bins without valid data in neighbouring range-bins, i.e. non-meteorological echoes that were not removed by the spectral clutter filter.

4. The specific differential phase, the differential backscatter phase, and their standard deviations are estimated according to [iv] but only for profiles that satisfy the following condition:
   $$\max\left[\Psi_{dp}(Z_{hh} > 25dBZ)\right] - \min\left[\Psi_{dp}(Z_{hh} > 25dBZ)\right] > 5deg,$$
   i.e. the differential phase (Ψ_{dp}) accumulation in rain should be at least 5 deg.
   The following coefficients were applied for the differential phases estimation, [iv]:
   a = 0.34 dB deg^{-1}, b = 0.055 dB deg^{-1}, d = 0.68, e = 0.042, f = 10 dBZ, g = 20 dBZ.

   Note: Because the differential backscatter phase is simply estimated as the difference of the measured differential phase and the differential propagation phase (which is twice the range accumulation of the specific differential phase), the knowledge of the precise system differential phase is required. The system differential phase is estimated according to [iv] and stored in the variable *differential_phase_offset*. In case the differential backscatter phase is biased, this offset can be checked in combination with the measured *differential_phase* available in [iii].

   In this processing step it is also checked whether total signal extinction and/or radar receiver saturation occurs, if so, *dataset_flags* will be set to the value *4*.

5. The reflectivity is corrected for gaseous (*gaseous_attenuation*) and rain attenuation as outlined in [v] (see Appendix B) and stored in the primary variable *equivalent_reflectivity_factor*.

6. The rainfall rate is estimated either based on a Z-R or KDP-R relation as outlined in [v] (see Appendix B).
   Dataset_flags shows, whether the rainfall rate is based on the Z-R (value *1*) or the KDP-R (value *2*) relation.

7. The standard deviation of the rainfall rate is estimated only when the KDP-R relation is applied as

$$\sigma_{\text{rain}} = c_2 \cdot \frac{\sigma_{kdp}}{K_{dp}} \cdot RR$$

   with the specific differential phase K_{dp}, its standard deviation σ_{kdp}, and the estimated rainfall rate $RR = c_1 \cdot K_{dp}^{c_2}$ (c_1 = 13, c_2 = 0.75) .

Data Quality

The raw signal streams of IDRA are processed in real-time by the radar control computer. Signal quality flags are not provided by the signal processing. Thus, users of this dataset should be aware of issues described in this Section.

It is strongly advised to consult the following resources which can help in identifying data quality issues with IDRA and its products:

- dataset quicklook of daily rain accumulation,
- http://ftp.tudelft.nl/TUDelft/irctr-rse/idra/ with all it's resources, i.e. animations of attenuated reflectivity plan-position indicators of the last years,
- measurements of the KNMI weather radar network which can be found online e.g. at http://www.buienradar.nl/historie.aspx (note that this website uses CET instead of UTC),
- rain gauge measurements at CESAR, i.e. the dataset *meteorological surface data, validated* which is available at the http://www.cesar-database.nl,
- measurements and quicklooks of the profiling radar TARA, i.e. the dataset *TARA processed multi-beam Doppler and polarimetric data* available at the CESAR database.

Clutter echoes (possible issue for Z-R relation only)

The signal processing employs a filtering of the polarimetric observables in the Doppler spectrum domain in order to suppress clutter echoes and interferences, [5]. However, some clutter (like insects in the summer time), and interference signatures might still be preserved in the processed data. These can be revealed by comparing IDRA data to other sensors, and sometimes also by inspecting rain accumulations based on IDRA's rainfall rate product (dataset quicklook). Usually, the remaining clutter is of weak amplitude and results in negligible rainfall rate estimates.

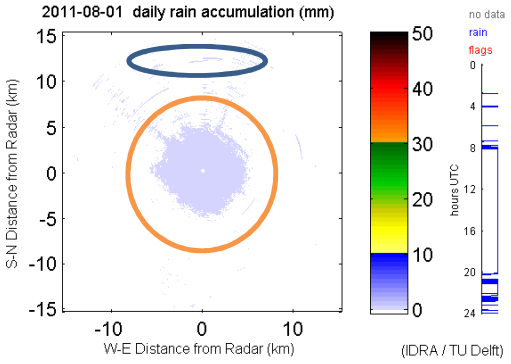

Figure 5: Possible clutter echoes, 2011-08-01.

Figure 5 shows the daily rain accumulation of the 1st of August 2011. The blue circle shows some remaining clutter from the highway A12. The orange circle highlights probably insects, they are measured only close to the radar because the radar sensitivity reduces with range. Usually insects are observed only during the day with its peak around noon, and only when ground temperatures raise above ~15°C.

Rainfall rate estimates based on the KDP-R relation are not sensitive to the clutter echoes described here.

Clutter filter (possible issue for Z-R relation only)

To suppress clutter echoes and interferences within the radar system, a notch filter in the Doppler domain is employed. Signals with Doppler velocities between -0.08 ms^{-1} and 0.08 ms^{-1} are suppressed.

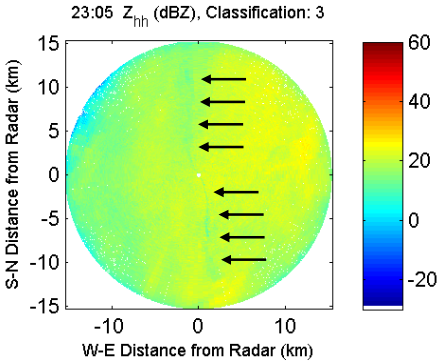

Figure 6: The effect of the (old signal processing) notch filter, 2008-08-03.

This also affects the estimated reflectivity in case when the radial velocity of the parts of the meteorological echo lays within the suppressed band of Doppler velocities. The resulting reduction of the reflectivity of the meteorological echo is perceivable in the PPI, see for an example Figure 6. However, it must be stressed that Figure 6 shows data with the old signal processing (before December 2009) where the notch filter was four times wider than in the current signal processing.

The clutter filter described here does not influence rainfall rate estimates based on the KDP-R relation.

Receiver Saturation

When the received echo exceeds the dynamic range of the radar receiver, saturation occurs. IDRA is equipped with an attenuator to reduce the transmitted power in these cases. This attenuator is however still not controlled automatically in real-time. Thus, the data might include receiver saturation effects that due to the nature of a FMCW radar results in a smearing effect in range.

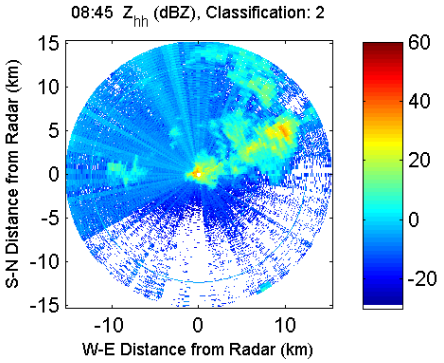

2009-06-04

Figure 7: The effect of receiver saturation on reflectivity measurements.

Figure 7 show examples of receiver saturation. In the data processing applied, usually regions of receiver saturation are identified and excluded from the rainfall rate retrieval, the primary variable *dataset_flags* can be used to check when and where this applies.

Multitrip echoes (possible issue for Z-R relation only)

In monostatic weather radar observations range aliasing can occur. In that case, the received signal stems from the transmission of an earlier sweep, and is thus designated to a wrong range closer to the radar. These multitrip echoes usually manifest in the PPI as radial reflectivity patterns with a low intensity as shown in Figure 8. Because of their low intensity, also the resulting estimated rainfall rates are weak.

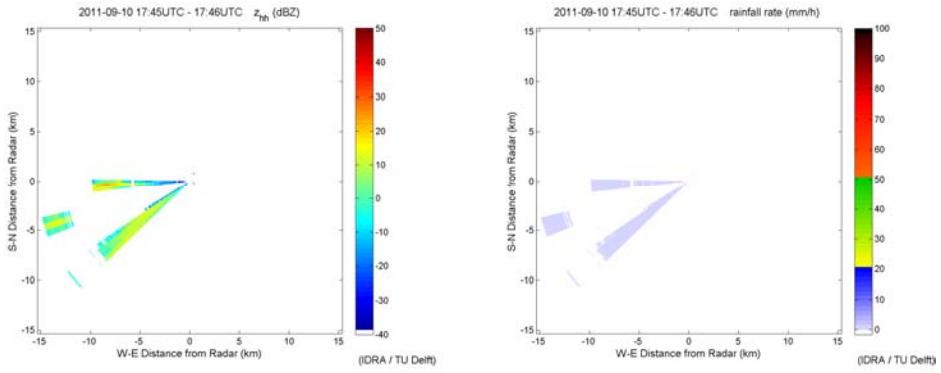

Figure 8: Multitrip echo, 2011-09-10.

Sometimes those multitrip echoes are not fully removed in this dataset. PPI's that do not contain an homogeneous precipitation pattern should thus be treated with care. Additionally one may also verify the presence of the multitrip echoes by evaluating the data of other instruments listed at the beginning of this section.

Synchronisation loss

For reasons that are still under investigation, a synchronisation loss occurs sometimes. This affects the computed weather radar observables. Figure 9 shows an example of such a corrupted reflectivity measurement. As for multitrip echoes, the PPI does not show an homogeneous precipitation pattern.

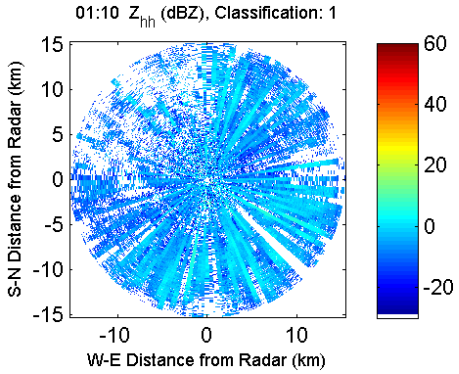

Figure 9: Corrupted IDRA reflectivity measurement due to the loss of synchronisation, 2009-06-04.

Usually when a synchronisation loss occurs, the data is not taken into account for rainfall rate retrieval because it is filtered out by the rain mask (step 1 of the data processing). Thus, if a synchronisation loss happened, rain echoes are missed by IDRA! You can use the resources introduced at the beginning of this section to check for such situations, i.e. comparing the rain mask on the quicklook with data of other sensors.

Melting layer

Based on the radiosounding (De Bilt) at 00:00UTC, 12:00UTC, and 24:00UTC, and the temperature measurements of the CESAR tower, the approximate lower height of the melting layer is estimated. Based on this estimate, a maximum range for IDRA measurements unaffected by the melting layer is calculated. *Dataset_flags* show when and where IDRA measurements are not considered for rainfall rate estimation due to possible melting layer contamination. This is also signalised on the quicklook (red curve).

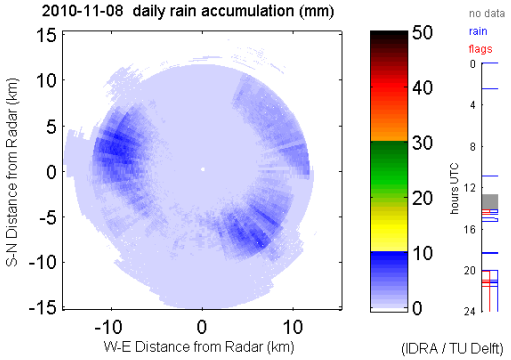

Figure 10: A low melting layer reduces the maximum range of rainfall rate estimation by IDRA, 2010-11-08.

Figure 10 shows a measurement where the rainfall rate retrieval is only carried out for a limited range due to a low melting layer. The quicklook of daily rain accumulation shows the clear cut-off at a range of about 10 km.

Note, that in the example of Figure 10 there still seem to be a range dependence of the daily rain accumulation which might indicate that parts of the melting layer were not correctly removed before rainfall estimation.

Instrument Details

Detailed Description

Figure 11 shows the block diagram of IDRA. The upper part of the figure shows the transmitter path. The lower part shows the co- and the cross-polarised receiver channels.

The synchronisation of the system is provided by a GPS timing board. This GPS timing board is also used to provide an accurate time stamp for the processed data.

For a detailed description of IDRA the reader is referred to [i].

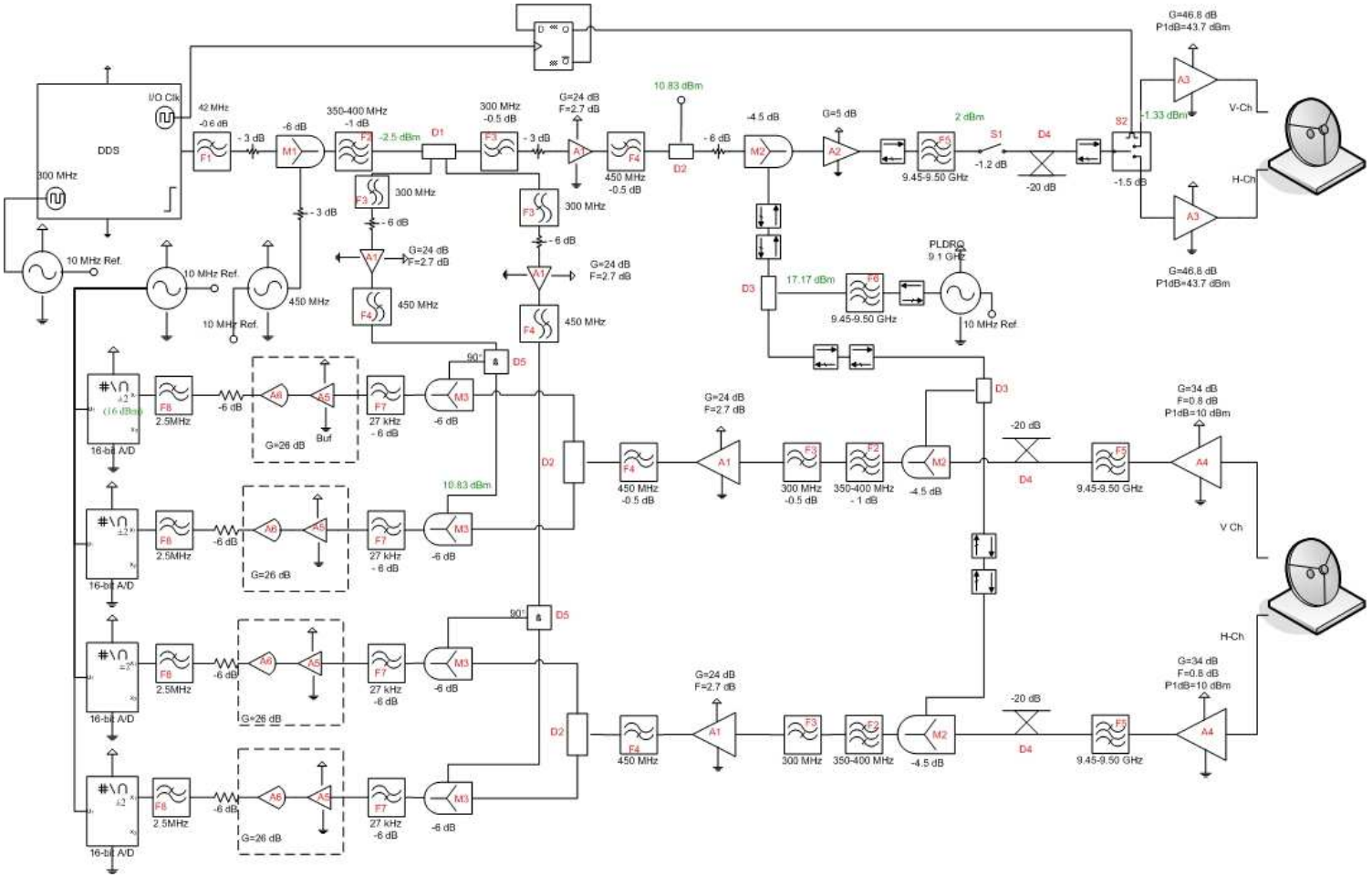

Figure 11: IDRA block diagram showing the transmitter and receiver channels.

Specifications

Table 2: Specifications of IDRA.

Parameter	Value	
latitude	51°58'11.92" North	
longitude	04°55'37.16" East	
Rijksdriehoekscoördinaten EPSG:28992 Amersfoort / RD New	x_{IDRA} = 123321 m y_{IDRA} = 442530 m	
height above sea-level	213 m agl.	
transmitter	solid-state amplifiers, modulation achieved by direct digital synthesiser	
polarisation on transmit	polarimetric (alternately linear horizontal and linear vertical)	
frequency modulation on transmit	sawtooth	
receiver	heterodyne, quadrature receiver, two channels, receiving the co- and the cross-polarised component (linear horizontal and linear vertical polarisation)	
maximum range	15 km in standard mode operation	
cross-polarisation isolation	< -30 dB	
minimum detectable reflectivity	-15 dBZ at 15 km	
dynamic range of the receiver	69 dB	
Parameter	**Symbol**	**Value**
central frequency	f_c	9.475 GHz
frequency excursion, the corresponding range resolution is $c/(2\cdot\Delta f)$	Δf	5 MHz
sweep time	ΔT	409.6 µs
transmitted power	P_t	0, 1, 2, 5, 10, 20 (W)
antenna gain, transmit	G_t	38.65 dB
antenna gain, receive	G_r	38.65 dB
gain of the receiver chain	G_{rec}	53 dB
antenna half-power beamwidth, transmit	θ_t	1.8° (0.031 rad)
antenna half-power beamwidth, receive	θ_r	1.8° (0.031 rad)

Theory of Operation

IDRA employs the frequency-modulated continuous wave radar principle, i.e. the radar is transmitting and receiving at the same time. The frequency of transmitted signal is sawtooth modulated. The backscattered and received echo is shifted in frequency with respect to the transmitted signal. This frequency shift, called the beat frequency, is directly related to the range of the echo.

The beat frequency is evaluated by mixing the transmitted signal with the received signal. Subsequently, a Fourier analysis is performed to separate the contributions from different range bins. The radar equation for distributed targets is then applied to calculate the reflectivity of each range bin.

For a detailed overview of the theory of operation, the reader is referred to [i].

Calibration

After IDRA has been built, extensive measurements have been carried out in order to characterise the system, and to derive the radar system constant necessary for accurate reflectivity measurements. For details about the calibration, the reader is again referred to [i]. In order to sustain the calibration of the system, a noise measurement is performed every day which is used to monitor variations of the receiver gain of IDRA.

In irregular intervals, passive measurements of the sun position is carried out in order to ensure that 0° azimuth corresponds to the Geographic North Pole.

Operation and Maintenance

More information about the operation and the maintenance of IDRA are available as internal documentation at TU Delft IRCTR.

Glossary and Acronyms

A/D	analogue-to-digital
CDS	CESAR database system
CESAR	Cabauw experimental site for atmospheric research
CET	Central European Time
dd	day
DDD	dataset description document
DDS	direct digital synthesizer
DOI	digital object identifier
FFT	fast Fourier transform
FMCW	frequency-modulated continuous-wave
GPS	global positioning system
HH	hour
IDRA	IRCTR drizzle radar
IRCTR	International Research Centre for Telecommunications and Radar of the Delft University of Technology
LDR	linear depolarisation ratio
MDD	metadata description document
mm	month
MM	minute
PI	principle investigator
PPI	plan position indicator
TARA	transportable atmospheric radar
yyyy	year
X-band	electromagnetic frequency band from 8 GHz to 12 GHz

Citable References

[i] J. Figueras i Ventura: "Design of a High Resolution X-band Doppler Polarimetric Weather Radar", *PhD Thesis*, TU Delft, 2009.
Available online at the institutional repository of TU Delft:
http://repository.tudelft.nl/view/ir/uuid%3Ad90b9ad6-237b-435d-9dc5-5660d9e7fbdd/

[ii] J. Figueras i Ventura and H. W. J. Russchenberg: "Towards a better understanding of the impact of anthropogenic aerosols in the hydrological cycle: IDRA, IRCTR drizzle radar", *Phys. Chem. Earth, Parts A/B/C*, vol. **34**, pp. 88 – 92.

[iii] T. Otto and H.W.J. Russchenberg, 2010: IDRA weather radar measurements – all data, TU Delft, Dataset, http://dx.doi.org/10.4121/uuid:5f3bcaa2-a456-4a66-a67b-1eec928cae6d.

[iv] T. Otto and H.W.J. Russchenberg: "Estimation of specific differential phase and differential backscatter phase from polarimetric weather radar measurements", *IEEE Geosci. Remote Sens. Lett.*, vol. **8**, pp. 988 – 992, 2011.

[v] T. Otto and H.W.J. Russchenberg: "Rainfall rate retrieval with IDRA, the polarimetric X-band radar at Cabauw, Netherlands", Proceedings of the 7th European Conference on Radar in Meteorology and Hydrology (ERAD 2012), Toulouse, France, June 2012.
A copy of this paper is provided in Appendix B.

References

[1] R. J. Doviak and D. S. Zrnić: “Doppler Radar and Weather Observations: Second Edition”, *Dover Publications*, 2006.

[2] H. Klein Baltink: “Cesar Database System – Metadata Description Document”, v0.7, KNMI, October 2007.

[3] H. Klein Baltink: “Cesar Database System – Interface Control Document”, v1.4, KNMI, August 2009.

[4] T. Otto: “Dataset Description Document for IDRA data in the 3TU.Datacentre”, 2010, http://data.3tu.nl/repository/uuid:9adbeb54-ce00-483e-abce-77a1229d84e8.

[5] C. Unal: “Spectral Polarimetric Radar Suppression to Enhance Atmospheric Echoes”, *J. Atmos. Oceanic Technol.*, vol. **26**, pp. 1781 – 1797, 2009.

[6] T. Otto and H.W.J. Russchenberg: “Estimation of the raindrop-size distribution at X-band using specific differential phase and differential backscatter phase”, *Proc. 6th European Conf. on Radar in Meteorology and Hydrology: Adv. in Radar Technology*, Sibiu, Romania, ISBN 978-973-0-09057-4, pp. 129 – 134, 2010.

[7] T. Otto and H.W.J. Russchenberg: "Advances in polarimetric X-band weather radar”, *Proceedings of the 9th European Radar Conference*, Amsterdam, Netherlands, ISBN 978-2-87487-029-3, pp. 174 – 177, 2012.

Appendix A: Header dump of the IDRA product dataset

```
netcdf cesar_idra_products_lb1_t00_v1.0_yyyymmdd.nc {

 dimensions:
   scalar = 1;
   time   = UNLIMITED;
   range  = 512;
   quicklook_azimuth = 143;

 variables:
   char iso_dataset(scalar=1);
     :title = "IDRA post-processed data: rainfall rate estimates and differential
               propagation and backscatter phases";
     :abstract = "This dataset contains post-processed X-band (central frequency of
                 9.475 GHz) weather radar data from the TU Delft IRCTR drizzle
                 radar IDRA. It includes plan-position indicators (PPI) of the
                 specific differential phase, the differential backscatter phase,
                 and the estimated rainfall rate. IDRA is mounted at the top of the
                 Cabauw tower at 213 m agl., and is scanning horizontally at a
                 fixed low elevation angle, covering a slant range of 15 km with a
                 range resolution of 30 m. IDRA thus provides the horizontally spa-
                 tial distribution of precipitation over the CESAR observatory.";
     :status = "onGoing";
     :hierarchyLevel = "dataset";
     :url = "http://www.cesar-database.nl";
     :protocol = "website";
     :uid_dataset = "2e590c10-2297-11e2-81c1-0800200c9a66";
     :topic = "climatologyMeteorologyAtmosphere";
     :keyword = "radar, differential phase, precipitation, rainfall rate";
     :westbound_longitude = "4.707";
     :eastbound_longitude = "5.145";
     :southbound_latitude = "51.835";
     :northbound_latitude = "52.105";
     :temporal_extent = "2010-01-01,onGoing";
     :datasetDate = "2012-11-01";
     :datasetDateType = "publication";
     :statement = "Based on the dual-polarimetric radar moments measured by IDRA,
                  the specific differential phase, the differential backscatter
                  phase and the rainfall rate are estimated.";
     :code = "28992";
     :codeSpace = "EPSG";
     :accessConstraints = "CESAR data policy";
     :useLimitation = "none";
     :organisationName_dataset = "Delft University of Technology (DUT)";
     :email_dataset = "t.otto@tudelft.nl";
     :role_dataset = "Principle Investigator";
     :metadata_id = "672c0380-2297-11e2-81c1-0800200c9a66";
     :organisationName_metadata = "Delft University of Technology (DUT)";
     :role_metadata = "Principle Investigator";
     :email_metadata = "t.otto@tudelft.nl";
     :url_metadata = "http://atmos.weblog.tudelft.nl";
     :metadataDate = "2012-11-01";
     :metadataDateType = "creation";
     :language = "eng";
     :metadataStandardName = "ISO-19115";
     :metadataStandardNameVersion = "Nederlands profiel op ISO 19115 voor
                                     geografie, v1.2";

   char product(scalar=1);
     :date_start_of_data = "2011-09-10T15:00:05Z";
     :ref_doc = "cesar_idra_products_lb1_t00_v1.0.pdf";
     :ref_doc_version = "1.0";
     :format_version = "netCDF,4.0";
     :originator = "Otto T., DUT";
     :revision_date = "2012-11-01";
     :radar_radiation_wavelength = "Central radiation wavelength (meter): 0.03164";
```

```
  :elevation_above_horizon = "Elevation (degree) measured from the horizon (0
                             degree) upwards: 0.5";
  :antenna_beam_width = "Half-power beam-width of the transmit and receive an-
                        tennas (degree): 1.8";
  :sweep_time = "Sweep time of the transmitted linear up-chirp (s-6): 409.6";
  :sample_size = "Number of sweeps that are averaged for the calculation of one
                 profile: 512";
  :date_end_of_data = "2011-09-10T15:59:58Z";

char station_details(scalar=1);
  :name = "CESAR observatory";
  :latitude = "51.97";
  :longitude = "4.926";
  :elevation = "-0.7";
  :WMO_id = "06348";
  :address = "Zijdeweg 1";
  :postal_code = "3411 MH";
  :city = "Lopik";
  :administration_area = "Utrecht";
  :country = "the Netherlands";

float time(time=2613);
  :standard_name = "time";
  :units = "hours since 2011-09-10 00:00:00";
  :axis = "T";

int range(range=512);
  :long_name = "slant_range";
  :cesar_standard_name = "slant_range";
  :scan_type = "non-fixed";
  :main_beam_elevation_above_horizon = 0.5f; // float
  :units = "m";
  :comment = "Slant range (meter) to the leading edge of the range bins. The ra-
             dial extension of the range bins is provided by the variable
             <range_resolution>.";

float quicklook_azimuth(quicklook_azimuth=143);
  :long_name = "Azimuth for the daily accumulated rainfall quicklook";
  :units = "rad";
  :comment = "The azimuth (radian) is measured clockwise from the Geographic
             North Pole.";

float azimuth(time=2613);
  :long_name = "azimuth";
  :units = "rad";
  :comment = "The azimuth (radian) is measured clockwise from the Geographic
             North Pole.";

short equivalent_reflectivity_factor(time=2613, range=512);
  :comment = "Co-polarised equivalent reflectivity factor at horizontal polari-
             sation in logarithmic units (dBZ, normalised to 1 mm6 m-3) correct-
             ed for gaseous and rain attenuation.";
  :_FillValue = -32768S; // short
  :units = "dBZ";
  :long_name = "reflectivity corrected for attenuation";
  :scale_factor = 0.0030518509475997192; // double

short specific_differential_phase(time=2613, range=512);
  :long_name = "specific differential phase";
  :units = "degree km-1";
  :scale_factor = 0.0061037018951994385; // double
  :comment = "Estimated specific differential phase KPD (degree km-1).";
  :_FillValue = -32768S; // short
```

```
short sigma_specific_differential_phase(time=2613, range=512);
  :long_name = "standard deviation of the specific differential phase";
  :units = "degree km-1";
  :scale_factor = 0.0061037018951994385; // double
  :comment = "Standard deviation of the estimated specific differential phase
              estimate due to measurement uncertainties only. Please refer to the
              dataset description document for details.";
  :_FillValue = -32768S; // short

short differential_backscatter_phase(time=2613, range=512);
  :long_name = "differential backscatter phase";
  :units = "degree";
  :scale_factor = 0.005493331705679495; // double
  :comment = "Estimated differential backscatter phase (degree).";
  :_FillValue = -32768S; // short

short sigma_differential_backscatter_phase(time=2613, range=512);
  :long_name = "standard deviation of the differential backscatter phase";
  :units = "degree";
  :scale_factor = 0.005493331705679495; // double
  :comment = "Standard deviation of the estimated differential backscatter phase
              due to measurement uncertainties only. Please refer to the dataset
              description document for details.";
  :_FillValue = -32768S; // short

short rainfall_rate(time=2613, range=512);
  :long_name = "instantaneous_rainfall_rate";
  :units = "mm h-1";
  :scale_factor = 0.01; // double
  :add_offset = 327.67; // double
  :comment = "Estimated rainfall rate based on the specific differential phase
              whenever available, else based on the reflectivity.";
  :_FillValue = -32768S; // short
  :_Unsigned = "true";

short sigma_rainfall_rate(time=2613, range=512);
  :long_name = "standard deviation of the instantaneous rainfall rate";
  :units = "mm h-1";
  :scale_factor = 0.01; // double
  :add_offset = 327.67; // double
  :comment = "Standard deviation of the estimated rainfall rate due to measure-
              ment uncertainties only. Please refer to the dataset description
              document for details.";
  :_FillValue = -32768S; // short
  :_Unsigned = "true";

byte dataset_flags(time=2613, range=512);
  :comment = "Dataset flags indicated regions where no rainfall rate estimation
              was possible due to total signal extinction, receiver saturation,
              or radar measurements possibly within or above the melting layer.";

float thickness_of_daily_rainfall_amount(quicklook_azimuth=143, range=512);
  :long_name = "daily accumulated rainfall";
  :units = "m";
  :comment = "Plan-position indicator of the daily accumulated rainfall as shown
              on the quicklook.";

float differential_phase_offset(time=2613);
  :long_name = "differential phase offset";
  :units = "rad";
  :comment = "Differential phase offset that was used for the calculation of the
              differential backscatter phase. Please refer to the dataset de-
              scription document for details.";
  :_FillValue = -999.0f; // float

float gaseous_attenuation(range=512);
  :long_name = "estimated gaseous attenuation";
  :units = "dB";
```

```
      :comment = "Gaseous attenuation used for the attenuation correction of the re-
                 flectivity.";
    int frequency_excursion(scalar=1);
      :long_name = "frequency excursion";
      :units = "s-1";
      :comment = "Frequency excursion of the transmitted linear up-chirp.";

    int range_resolution(scalar=1);
      :long_name = "range resolution";
      :units = "m";
      :comment = "Radial extension (meter) of one range bin.";

  :title       = "IDRA post-processed data: rainfall rate estimates and differential
                 propagation and backscatter phases";
  :institution = "Delft University of Technology (DUT)";
  :history     = "Based on the dual-polarimetric radar moments measured by IDRA, the
                 specific differential phase, the differential backscatter phase
                 and the rainfall rate are estimated.";
  :references  = "cesar_idra_products_lb1_t00_v1.0.pdf @ http://www.cesar-
                 database.nl";
  :Conventions = "CF-1.4";
  :location    = "CESAR observatory, the Netherlands";
  :source      = "Ground-based polarimetric weather radar";
  :example     = "http://ftp.tudelft.nl/TUDelft/irctr-rse/idra/";
}
```

Appendix B: Rainfall rate retrieval with IDRA

ERAD 2012 - THE SEVENTH EUROPEAN CONFERENCE ON RADAR IN METEOROLOGY AND HYDROLOGY

Rainfall rate retrieval with IDRA, the polarimetric X-band radar at Cabauw, Netherlands

Tobias Otto

Tobias Otto and Herman W.J. Russchenberg
TU Delft Climate Institute, Department of Geoscience and Remote Sensing, Stevinweg 1, 2628CN Delft, Netherlands, t.otto@tudelft.nl, h.w.j.russchenberg@tudelft.nl
(Dated: 30 May 2012)

Abstract

In 2012, a polarimetric X-band weather radar will be installed in the city of Rotterdam in the frame of the INTERREG IVB NWE programme RAINGAIN[1]. The purpose of this radar is the measurement of rainfall rate with a high spatial and temporal resolution to allow the urban water management authorities to cope with extreme rainfall events and to help preventing flood damage.

In order to define an optimum rainfall rate retrieval algorithm for the Rotterdam radar, we evaluate in this contribution a rainfall rate retrieval algorithm based on differential phase measurements. For this study, we are using data acquired by the polarimetric X-band radar IDRA which is operated since 2007 at the Dutch national meteorological observatory CESAR[2].

1. Introduction

Weather radars are common to measure the spatial distribution and the temporal evolution of precipitation over a wide range. The operational weather radar network of Europe (EUMETNET/OPERA Radar Network) that covers the whole of Europe currently consists of 194 radars working at S- and C-band[3]. Those radars provide a low elevation precipitation scan with a spatial and temporal resolution down to 1x1 km² every 5 minute. This coarse resolution is a result of the sparse placement of these radars, and the volume scanning strategy that is required to accommodate the multitude of stakeholders such as weather fore- and now-casters, aviation meteorologists, and hydrologists.

In recent years, radar meteorologists exploit X-band weather radars for dedicated, short-range (<50 km) applications as:

- gap-filling radars in complex terrain such as mountainous areas, Météo France Dossier de Presse (2011),
- to obtain high-resolution rainfall data in densely populated urban areas for the improvement of urban water management and flood prediction, Maki et al. (2008), RAINGAIN project[1],
- to improve the low-altitude radar coverage, McLaughlin et al. (2009).

The compactness of X-band weather radars makes them easily deployable even in urban areas. Furthermore, they can provide a higher temporal and spatial resolution than standard operational weather radars because of the reduced range coverage, and the less stringent requirements on the scanning strategy due to their focused application.

However, the *X-band challenge* for the observation of precipitation is the significant higher level of attenuation by rain. Cloudbursts with instantaneous rainfall rates >100 mmh^{-1} may even lead to the total extinction of the radar signal within few kilometres. One way to counteract on the attenuation issue is the use of polarimetric radars at linear horizontal / vertical polarisation basis. Such radars can directly measure the differential phase, i.e. the phase difference between the co-polarised echoes at horizontal and vertical polarisation. The differential phase is a self-calibrating measurement, and, furthermore, it is not affected by attenuation unless the radar signal is totally extinct. However, because the scattering regime at X-band can be non-Rayleigh already in moderate rain, the differential phase is a superposition of the differential phase on propagation and on backward-scattering. In Otto and Russchenberg (2011), we proposed a method to estimate the range derivative of the differential propagation phase, the specific differential phase K_{dp}, and the differential backscatter phase δ_{co}. By reflectivity-weighting, this method also achieves an improved range resolution compared to conventional K_{dp} estimators. In this contribution we applied this method for the estimation of K_{dp} and in turn for the estimation of the rainfall rate. The polarimetric weather radar terminology and the scattering computation methodology are introduced in the next section followed by a detailed description of the rainfall rate estimation algorithm. Finally, the rainfall rate is estimated for an IDRA rain measurement in September 2011, and some conclusions are drawn.

2. Basics

Usual polarimetric weather radar observables include the reflectivities $Z^{att}_{hh,vv}$ based on the co-polarised echoes at horizontal (*hh*) and vertical (*vv*) polarisation, and the differential phase $\Psi^{2\text{-way}}_{dp}$:

$$Z^{att}_{hh,vv}(r_n) = Z_{hh,vv}(r_n) - 2\int_{r_1}^{r_{n-1}} \alpha^{1\text{-way}}_{hh,vv}(r)dr \qquad (1)$$

[1] http://www.raingain.eu.
[2] CESAR – Cabauw Experimental Site for Atmospheric Research, http://www.cesar-observatory.nl.
[3] OPERA – Operational Programme for the Exchange of Weather Radar Information, "Radar database v1.17", http://www.knmi.nl/opera, March 2012.

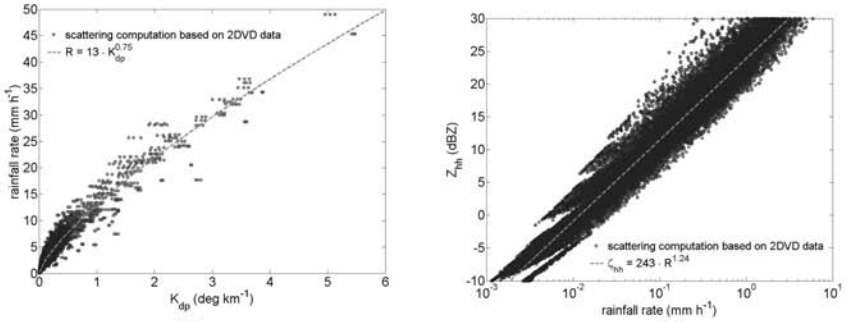

Fig. 1: Relationships used for the rainfall rate estimation at X-band based on scattering computations using 41530 RDSD's measured by a 2D video distrometer throughout the year 2009 at Cabauw and corresponding fits: (a) rainfall rate vs. K_{dp}, (b) Z_{hh} vs. rainfall rate for $Z_{hh} \leq 30$dBZ.

$$\Psi_{dp}^{2\text{-way}}(r_n) = \delta_{co}(r_n) - 2\int_{r_1}^{r_{n-1}} K_{dp}(r)dr \quad . \tag{2}$$

The first term in (1) and (2), i.e. the intrinsic reflectivities $Z_{hh,vv}$ and the differential backscatter phase δ_{co} stem from the backward-scattering in the range-bin r_n. The second terms consisting of the specific attenuations $\alpha_{hh,vv}^{1\text{-way}}$ and the one-way specific differential phase K_{dp} are due to the propagation of the radar signal from the radar at range r_1 to the leading edge of the range bin r_n. In case of rain, all terms in (1) and (2) can be related to the raindrop-size distribution (RDSD) $N(D)$:

$$\zeta_{hh,vv} = \frac{\lambda^4}{\pi^5 |K|^2} 10^{18} \int_D \sigma_{hh,vv}(D) N(D) dD \tag{3}$$

$$\alpha_{hh,vv}^{1\text{-way}} = 8.686 \cdot 10^3 \cdot \lambda \int_D \Im\left[f_{hh,vv}(D) \right] N(D) dD \tag{4}$$

$$\delta_{co} = \arg\left[\int_D s_{hh}^*(D) s_{vv}(D) N(D) dD \right] \tag{5}$$

$$K_{dp} = \frac{180}{\pi} 10^3 \cdot \lambda \int_D \Re\left[f_{hh}(D) - f_{vv}(D) \right] N(D) dD \, . \tag{6}$$

In (3) - (6), D is the equivolumetric raindrop diameter, λ is the wavelength, $|K|^2$ the dielectric factor, $\sigma_{hh,vv}=4\pi|s_{hh,vv}|^2$ are the radar cross sections at linear horizontal and linear vertical polarisation with $s_{hh,vv}$ and $f_{hh,vv}$ representing the backward- and the forward-scattering amplitudes of the hydrometeors, respectively. The reflectivity is usually displayed in logarithmic units

$$Z_{hh,vv}(\text{dBZ}) = 10 \log_{10}\left(\frac{\zeta_{hh,vv}}{1\text{mm}^6\text{m}^{-3}} \right). \tag{7}$$

For scattering computations, we obtain numerical values of the forward- and backward-scattering amplitudes for rain using the Fredholm integral method, Holt et al. (1978), with the model for the complex refractive index of water given by Liebe et al. (1991). Three oblate, spheroidal raindrop shape models were used: Brandes et al. (2005), Thurai et al. (2007), and a combination of Keenan et al. (2001) for D < 1.35 mm, Andsager et al. (1999) for 1.35 mm ≤ D ≤ 4.4 mm, and Beard and Chuang (1987) for D > 4.4 mm (KAB). To properly represent the natural variability of rain, we use 41530 RDSD's measured by a 2D video-disdrometer throughout the year 2009 at Cabauw, Leijnse et al. (2010). To include also variations of the raindrop temperature, the air temperature at 1.5 m height measured operationally at Cabauw was used.

The following section introduces an algorithm to invert of the radar measurements, specifically the reflectivity and the specific differential phase, in order to estimate the rainfall rate.

Rainfall rate estimation

The radar observables introduced in the previous section can be linked to the rainfall rate which in turn is given by

$$R = \frac{3.6}{10^3} \cdot \frac{\pi}{6} \cdot \int_D v(D) D^3 N(D) dD \tag{8}$$

with $v(D)$ the raindrop terminal velocity. Traditionally, only the reflectivity is used to estimate the rainfall rate because it was the only measurement that the first weather radars could obtain. However, the reflectivity is not the most favourable choice because it is prone to radar signal attenuation and to radar mis-calibration which might corrupt the rainfall rate estimates. A polarimetric weather radar measurement that is not affected by these issues is the differential phase, (2). At X-band in moderate to strong rain non-Rayleigh scattering may occur with the result that the differential phase is not only the range accumulation of the specific differential phase K_{dp}, (6), but it is superposed by the differential backscatter phase δ_{co},

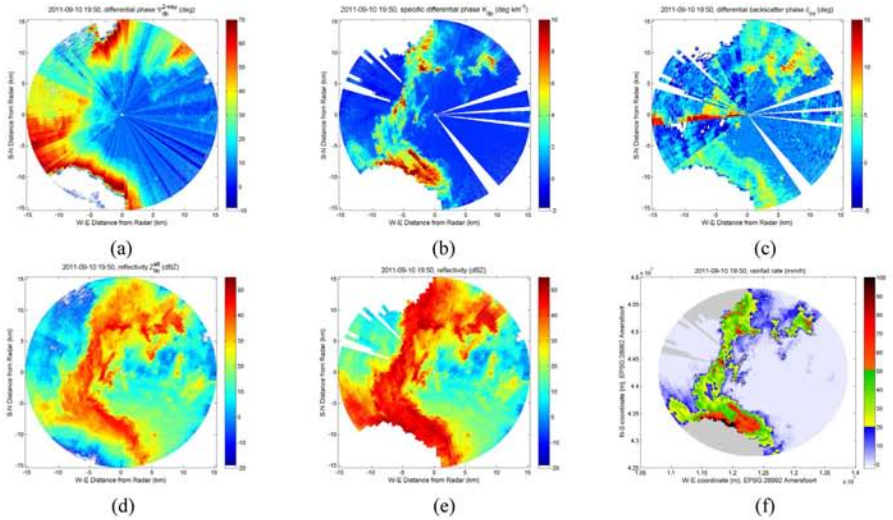

Fig. 2: For the IDRA measurement (2011-09-10 19:50UTC) plan position indicators are shown of (a) the measured differential phase $\Psi_{dp}^{2\text{-way}}$ (deg) which is decomposed into (b) the specific differential phase K_{dp} (deg km^{-1}) and (c) the differential backscatter phase δ_{co}. K_{dp} is used with (10) to correct (d) the measured reflectivity Z_{hh}^{att} (dBZ) for attenuation resulting in (e) Z_{hh} (dBZ). K_{dp} and Z_{hh} are used for the estimation of (f) the instantaneous rainfall rate (mm h^{-1}) as explained in the text. Note that (a)-(e) show the data in the radar-centred polar coordinate system (30 m range resolution) while for (f) the data is mapped to the RD New coordinates with a spatial resolution of 100x100 m. Grey-shaded areas in (f) show regions where the radar data is flagged as unavailable due to receiver saturation or total radar signal extinction.

(5). In such cases, methods like Hubbert and Bringi (1995), Otto and Russchenberg (2011) can be applied to separate K_{dp} and δ_{co}. Next we describe how K_{dp} is used in the context of quantitative precipitation estimation (QPE) for the TU Delft IRCTR drizzle radar (IDRA), Figueras i Ventura and Russchenberg (2009).

Before the rainfall rate estimation, the radar data undergoes pre-processing steps which for IDRA comprise spectral processing including a polarimetric spectral clutter suppression, Unal (2009), and estimation of the polarimetric weather radar observables as outlined by Figueras i Ventura (2009, Section 4.2.7). Range segments of receiver saturation and total radar signal extinction are detected and removed from further data processing. We then separate profile-by-profile the forward- and backward-scattering components of the reflectivity and the differential phase. First K_{dp} and δ_{co} are estimated, Otto and Russchenberg (2011), when the following condition is met

$$\max(\Psi_{dp}) - \min(\Psi_{dp})\Big|_{Z_{hh}^{att} > 25dBZ} > 5\,\text{deg}\,. \tag{9}$$

K_{dp} is used to estimate the specific attenuation at horizontal polarisation, Holt (1988), applying the linear relation

$$\alpha_{hh}^{1\text{-way}} = 0.34 \cdot K_{dp} \tag{10}$$

with $\alpha_{hh}^{1\text{-way}}$ (dB km^{-1}) and K_{dp} (deg km^{-1}). This relation is valid for X-band (9.475 GHz) and has been determined by scattering computations as outlined in the previous section. In case that the differential phase accumulation for one profile does not exceed the threshold defined in (9), the attenuation is estimated by

$$\alpha_{hh}^{1\text{-way}} = 2.82 \times 10^{-5} \cdot 10^{Z_{hh}^{att}/10} \tag{11}$$

with $\alpha_{hh}^{1\text{-way}}$ (dB km^{-1}) and Z_{hh}^{att} (dBZ). Also this relation is valid for X-band (9.475 GHz) and has been determined by scattering computations taking only reflectivities equal to or less than 30 dBZ into account. We also account for gaseous attenuation applying (3.19) from Doviak and Zrnić (1993).

For the estimation of the rainfall rate R the following relations are applied

$$R = 13 \cdot K_{dp}^{0.75} \tag{12}$$

$$\zeta_{hh} = 243 \cdot R^{1.24} \quad \text{valid for } Z_{hh} \le 30\ \text{dBZ} \tag{13}$$

with R (mm h^{-1}), K_{dp} (deg km^{-1}) and ζ_{hh} (mm^6 m^{-3}). The result of the scattering computations that have been used to determine (12) and (13) are displayed in Fig. 1. The raindrop terminal fall velocity relation given by Atlas et al. (1973) has been employed. Note that (13) is only valid for reflectivities equal to or less than 30 dBZ. Finally, for the estimation of the

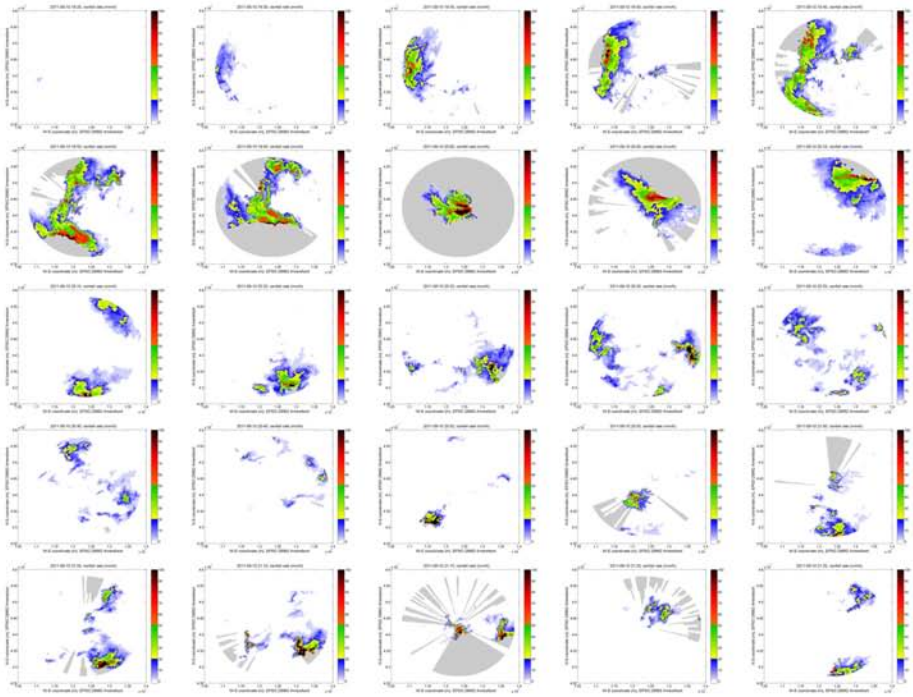

Fig. 3: Temporal evolution of the case study showing the IDRA rainfall rate estimate every 5 minutes. Note that IDRA is constantly rotating at a fixed low elevation angle, providing an update of the rainfall rate once per minute.

rainfall rate, (12) is used whenever K_{dp} is available, its standard deviation is less than 2 deg km^{-1} and $Z_{hh} > 30$ dBZ, else (13) is used.

As a last step, the rainfall rate is mapped from the radar-centred polar coordinate system to the Dutch Rijksdriehoekscoördinaten EPSG 28992 Amersfoort (RD New) with a spatial resolution of usually 100x100 m and a temporal resolution of 1 minute.

Heavy rain case study 2011-09-10

To test the rainfall rate retrieval as outlined in the previous section, we applied the method to IDRA data from 2011-09-10 19:00-21:30UTC where IDRA measured heavy precipitation as a result of a cold front passing over the Netherlands. The polarimetric X-band radar IDRA (1 round per minute) is placed on top of the 213 m high meteorological tower at CESAR, Fig. 4(a), and is scanning continuously with 1 round per minute at a fixed low elevation angle of 0.5 deg. For this measurement, IDRA which is a frequency-modulated continuous wave radar was set to its standard mode with a sweep time of 409.6 µs and a frequency excursion of 5Mhz which results in 512 range bins with a range resolution of 30 m, i.e. 15.36 km maximum range.

Fig. 2 shows plan position indicators of the IDRA measurement at 19:50UTC, specifically, Fig. 2(a) shows the measured differential phase $\Psi_{dp}^{2\text{-way}}$ (deg) which is decomposed into Fig. 2(b) the specific differential phase K_{dp} (deg km^{-1}) and Fig. 2(c) the differential backscatter phase δ_{co}. K_{dp} is used with (10) to correct Fig. 2(d) the measured reflectivity Z_{hh}^{att} (dBZ) for attenuation resulting in Fig. 2(e) Z_{hh} (dBZ). K_{dp} and Z_{hh} are then used for the estimation of Fig. 2 (f) the instantaneous rainfall rate (mm h^{-1}) as explained in previous section. Note that Fig. 2(a)-(e) show the data in the radar-centred polar coordinate system (30 m range resolution) while for Fig. 2(f) the data is mapped to the RD New coordinates with a spatial resolution of 100x100 m. Grey-shaded areas in Fig. 2(f) show regions where the radar data is flagged as unavailable due to receiver saturation or total radar signal extinction. Fig. 2(b) shows that due to the strength of this precipitation event, K_{dp} is almost everywhere available. Note also the high spatial resolution of K_{dp} compared to conventional estimators which is achieved by reflectivity-weighting based on the self-consistency principle, Otto and Russchenberg (2011). The high spatial resolution of K_{dp} translates directly into a high spatial resolution of the rainfall rate estimate.

Fig. 3 shows the rainfall rate estimates for this event in time steps of five minutes. However, note that not all data is shown due to space constraints; IDRA is providing a higher temporal resolution of one minute. From Fig. 3 (20:00UTC) it is evident that attenuation poses a major limitation in heavy precipitation for an effective rainfall rate estimation over larger

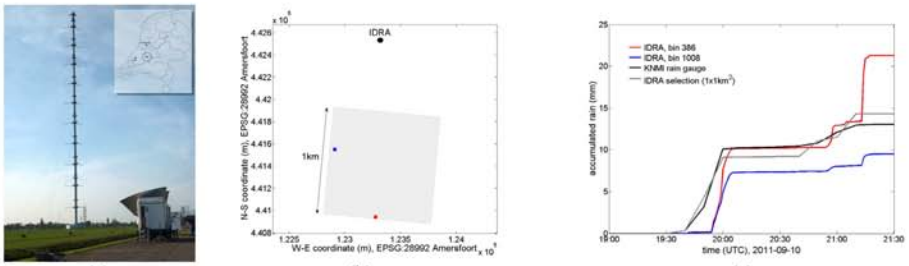

(a) (b) (c)

Fig. 4: (a) Photo of the two TU Delft radar (profiling S-band radar TARA, and scanning X-band radar IDRA on top of the tower) at CESAR, (b) selection of a 1x1 km² area 500 m south of IDRA divided into a grid of 30x30 m, and (c) accumulated rain for the case study 2011-09-10 measured by IDRA and the KNMI rain gauge.

areas at X-band. Therefore, instead of a stand-alone installation of an X-band weather radar for QPE, a network of X-band radars should be favoured, or the X-band measurements need to be complemented in heavy precipitation with data from the operational weather radar network.

To fully exploit the high-spatial resolution of IDRA, we mapped the rainfall rate within the 1x1km² area south of IDRA shown in Fig. 4(b) onto a grid of 30x30 m resolution. For the selected case study, Fig. 4(c) shows the rain accumulation for:

- the KNMI rain gauge which is placed close to IDRA (black curve),
- the IDRA rainfall rate estimate averaged in space over the 1x1km² shown in Fig. 4(b) and in time to match the temporal resolution (10 minutes) of the KNMI rain gauge (grey curve),
- the IDRA rainfall rate for the blue 30x30 m grid point highlighted in Fig. 4(b) (blue curve),
- the IDRA rainfall rate for the red 30x30 m grid point highlighted in Fig. 4(b) (red curve).

From Fig. 4(c) it can be seen that the in space and time averaged IDRA rainfall rate estimate (grey curve) fits very well with the KNMI rain gauge measurement (black curve) although the rain gauge is placed close to IDRA and not within the 1x1 km² area shown in Fig. 4(b). The difference of rain accumulation at 21:30UTC is only about 1.3 mm which provides confidence in the rainfall rate estimation outlined in the previous section, this good match between IDRA and the rain gauge was also confirmed for other rainfall events by Bruni et al. (2012).

The red and the blue curve in Fig. 4(c) show the rain accumulation from the 30x30 m grid points highlighted in Fig. 4(b). Although the grid points are only about 700 m apart, the rain accumulation at 21:30UTC differs by 11.8 mm. One of the reasons for this is certainly the high spatial and temporal variability of this event, Fig. 3. It therefore suggests the need for high-resolution radar observations both in space and time especially for hydrological applications in urban water management and flood prediction in cities at street scale. Also, due to the temporal variability, a strong precipitation core might not be sampled at a specific location because of the low revisit time of IDRA of one minute. Thus, it might be beneficial to link the rainfall rate estimation to a storm-tracking algorithm or to setup adaptive scanning strategies for such dynamic precipitation events.

Conclusions

In this contribution, we presented a rainfall rate estimation algorithm for IDRA, the scanning, polarimetric X-band radar at CESAR. The algorithm is based on a high spatial resolution estimate of the specific differential phase whenever it is available to avoid issues such as radar calibration or attenuation. The algorithm is not final yet; it misses a hydrometeor classification and a melting layer height detection. However, most of the time, IDRA is measuring in rain due to the low elevation angle, the limited range of 15 km in the standard mode and the moderate temperatures in the Netherlands.

We applied the algorithm successfully to a heavy rain case study in September 2011. The accumulated rain over a period of 2.5h averaged in space and time of IDRA matches well a co-located rain gauge measurement. However, further validation is required. For this event, a high spatial and temporal variability was observed which confirms the demand for high-resolution precipitation measurements, e.g. by X-band radars for dedicated purposes such as the rainfall rate estimation at street scale in urban environments for flood prediction and as an input to urban drainage models. To further improve high-resolution QPE, adaptive scanning strategies and rainfall rate estimation linked to storm-tracking algorithms should be investigated.

Later this year we will start to process all IDRA data collected so far with this algorithm, and to make the estimated rainfall rate freely available online at *http://www.cesar-database.nl* and *http://data.3tu.nl/repository/collection:cabauw*.

Acknowledgment

This study was supported by the INTERREG IVB NWE project RAINGAIN. The authors acknowledge the KNMI for providing the meteorological surface data at CESAR (available online at http://www.cesar-database.nl). We also thank Fred van der Zwan and Paul Hakkart for their technical support in operating IDRA.

References

Andsager K., Beard K.V., Laird N.F., 1999: Laboratory Measurements of Axis Ratios for Large Raindrops, *J. Atmos. Sci.*, **56**, 2673-2683.

Atlas D., Srivastava R.C., Sekhon R.S., 1973: Doppler Radar Characteristics of Precipitation at Vertical Incidence, *Rev. Geophys.*, **11**, 1-35.

Beard K.V., Chuang C., 1987: A New Model for the Equilibrium Shape of Raindrops, *J. Atmos. Sci.*, **44**, 1509-1524.

Brandes E.A., Zhang G., Vivekanandan J., 2005: Corrigendum, *J. Appl. Meteor.*, **44**, 186.

Bruni G., ten Veldhuis J.A.E., Otto T., Leijnse H., 2012: Rainfall resolution from weather radars and their application in urban drainage modelling, *Geophysical Research Abstracts*, **14**, EGU General Assembly 2012, EGU2012-3317.

Doviak R.J., Zrnić D.S., 1993: Doppler Radar and Weather Observations, 2nd edition, *Academic Press*.

Figueras i Ventura J., Russchenberg H. W. J., 2009: Towards a better understanding of the impact of anthropogenic aerosols in the hydrological cycle: IDRA, IRCTR drizzle radar. *Phys. Chem. Earth, Parts A/B/C*, **34**, 88 – 92.

Figueras i Ventura J., 2009: Design of a High Resolution X-band Doppler Polarimetric Radar, *PhD thesis*, TU Delft, available online at http://repository.tudelft.nl/view/ir/uuid%3Ad90b9ad6-237b-435d-9dc5-5660d9e7fbdd/.

Holt A.R., Uzunoglu N.K., Evans B.G., 1978: An integral equation solution to the scattering of electromagnetic radiation by dielectric spheroids and ellipsoids, *IEEE Trans. Antennas Propag.*, **AP-26**, 706-712.

Holt A.R., 1988: Extraction of differential propagation phase from data from S-band circularly polarised radar, *Electron. Lett.*, **24**, 1241-1244.

Hubbert J., Bringi V.N., 1995: An Iterative Filtering Technique for the Analysis of Copolar Differential Phase and Dual-Frequency Radar Measurements, *J. Atmos. Oceanic Technol.*, **12**, 643-648.

Keenan T.D., Carey L.D., Zrnić D.S., May P.T., 2001: Sensitivity of 5-cm Wavelength Polarimetric Radar Variables to Raindrop Axial Ratio and Drop Size Distribution, *J. Appl. Meteor.*, **40**, 526-545.

Leijnse H., co-authors, 2010: Precipitation Measurement at CESAR, the Netherlands, *J. Hydrol.*, **11**, 1322-1329.

Liebe H.J., Hufford G.A., Manabe T., 1991: A model for the complex permittivity of water at frequencies below 1 THz, *Int. J. Infrared Millim. Waves*, **12**, 659-675.

Maki M., co-authors, 2008: X-band Polarimetric Radar Network in the Tokyo Metropolitan Area: X-NET, *Proceedings of ERAD2008, The Fifth European Conference on Radar in Meteorology and Hydrology*.

McLaughlin D., co-authors, 2009: Short-wavelength technology and the potential for distributed networks of small radar systems, *B. Am. Meteorol. Soc.*, **90**, 1797-1817.

Météo France Dossier de Presse, 2011: Présentation du premier radar du réseau RHyTMME.

Otto T., Russchenberg H.W.J., 2011: Estimation of Specific Differential Phase and Differential Backscatter Phase from polarimetric Weather Radar Measurements of Rain, *IEEE Geosci. Remote Sens. Lett.*, **8**, 988-992.

Thurai M., Huang G.J., Bringi V.N., Randeu W.L., Schönhuber M., 2007: Drop Shapes, Model Comparisons, and Calculations of Polarimetric Radar Parameters in Rain, *J. Atmos. Oceanic Technol.*, **24**, 1019-1032.

Unal C., 2009: Spectral Polarimetric Radar Clutter Suppression to Enhance Atmospheric Echoes, *J. Atmos. Oceanic Technol.*, **26**, 1781-1797.